

Spectral Energy Distributions and Light Curves of GRB 990123 and its Afterglow

T.J. Galama¹, M.S. Briggs², R.A.M.J. Wijers³, P.M. Vreeswijk¹, E. Rol¹, D. Band⁴, J. van Paradijs^{1,2}, C. Kouveliotou^{5,6}, R.D. Preece², M. Bremer⁷, I.A. Smith⁸, R.P.J. Tilanus⁹, A.G. de Bruyn^{10,11}, R.G. Strom^{1,10}, G. Pooley¹², A.J. Castro-Tirado^{13,14}, N. Tanvir^{15,16}, C. Robinson¹⁷, K. Hurley¹⁸, J. Heise¹⁹, J. Telting²⁰, R.G.M. Rutten²⁰, C. Packham²⁰, R. Swaters¹¹, J.K. Davies⁹, A. Fassia²¹, S.F. Green²², M.J. Foster²², R. Sagar²³, A.K. Pandey²³, Nilakshi²³, R.K.S. Yadav²³, E.O. Ofek²⁴, E. Leibowitz²⁴, P. Ibbetson²⁴, J. Rhoads²⁵, E. Falco²⁶, C. Petry²⁷, C. Impey²⁷, T.R. Geballe²⁸, D. Bhattacharya²⁹

1. Astronomical Institute 'Anton Pannekoek', University of Amsterdam, & Center for High Energy Astrophysics, Kruislaan 403, 1098 SJ Amsterdam, The Netherlands
2. Physics Department, University of Alabama in Huntsville, Huntsville AL 35899, USA
3. Department of Physics and Astronomy, SUNY Stony Brook, NY 11794-3800, USA
4. CASS, University of California in San Diego, La Jolla, CA 92093, USA
5. Universities Space Research Association
6. NASA/MSFC, Code ES-84, Huntsville AL 35812, USA
7. Institut de Radio Astronomie Millimétrique, 300 rue de la Piscine, F-38406 Saint-Martin d'Hères, France
8. Department of Space Physics and Astronomy, Rice University, MS-108, 6100 South Main, Houston, TX 77005-1892 USA
9. Joint Astronomy Centre, 660 North A'ohoku Place, University Park, Hilo, HI 96720, USA
10. NFRA, Postbus 2, 7990 AA Dwingeloo, The Netherlands
11. Kapteyn Astronomical Institute, Postbus 800, 9700 AV, Groningen, The Netherlands
12. Mullard Radio Astronomy Observatory, Cavendish Laboratory, University of Cambridge, Madingley Road Cambridge CB3 0HE, UK
13. Laboratorio de Astrofísica Espacial y Física Fundamental (LAEFF-INTA), P.O. Box 50727, E-28080 Madrid, Spain
14. Instituto de Astrofísica de Andalucía (IAA-CSIC), P.O. Box 03004, E-18080 Granada, Spain
15. Institute of Astronomy, Madingley Road, Cambridge CB3 0HA, UK
16. Department of Physical Sciences, University of Hertfordshire, College Lane, Hatfield, Herts AL10 9AB, UK
17. National Science Foundation
18. University of California at Berkeley, Space Sciences Laboratory, Berkeley, CA, USA 94720-7450
19. Space Research Organisation Netherlands (SRON), Sorbonnelaan 2, 3584 CA Utrecht,

The Netherlands

20. Isaac Newton Group, Apartado de Correos, 321, 38780 Santa Cruz de La Palma, Islas Canarias, Spain
21. Astrophysics Group, Blackett Laboratory, Imperial College, Prince Consort Road, London SW7 2BZ
22. Unit for Space Sciences and Astrophysics, School of Physical Sciences, Physics Laboratory, University of Kent at Canterbury, Canterbury, Kent, CT2 7NR, UK
23. U.P. State Observatory, Nainital
24. Wise Observatory, Tel Aviv University, Ramat Aviv, Tel Aviv 699 78, Israel
25. Kitt Peak National Observatory, 950 N. Cherry Avenue, P.O.O. Box 26732, Tucson, AZ 85726 USA
26. Harvard-Smithsonian Center for Astrophysics, Cambridge, MA 02138, USA
27. Steward Observatory, University of Arizona, Tucson AZ 85719, USA
28. Gemini Observatory, 670 N. A’ohoku Place, University Park, Hilo, HI 96720 USA
29. Raman Research Institute, Bangalore 560 080, India

This manuscript has been accepted for publication in Nature. The article is under embargo until publication. We do place restrictions on any dissemination in the popular media. You are free to refer to this paper in your own publications. For further enquiries, please contact Titus Galama (titus@astro.uva.nl) or Michael Briggs (briggs@gibson.msfc.nasa.gov).

Gamma-ray bursts (GRBs) are thought to result from the interaction of an extremely relativistic outflow interacting with a small amount of material surrounding the site of the explosion. Multi-wavelength observations covering the γ -ray to radio wavebands allow investigations of this ‘fireball’ model. On 23 January 1999 optical emission was detected while the γ -ray burst was still underway. Here we report the results of γ -ray, optical/infra-red, sub-mm, mm and radio observations of this burst and its afterglow, which indicate that the prompt and afterglow emissions from GRB 990123 are associated with three distinct regions in the fireball. The afterglow one day after the burst has a much lower peak frequency than those of previous bursts; this explains the short-lived nature of the radio emission, which is not expected to reappear. We suggest that such differences reflect variations in the magnetic-field strengths in the afterglow emitting regions.

1. INTRODUCTION

The current ‘industry standard’ model for γ -ray bursts and their afterglows is the fireball-plus-blastwave model (see Ref. 1 for a review). It invokes the release of a large amount of energy, of order $M_{\odot}c^2$, into a volume less than 1 light-msec across. This leads to a ‘fireball’ that expands ultra-relativistically (Lorentz factor $\Gamma \gtrsim 300$); when it runs into the surrounding medium a ‘forward shock’ ploughs into the medium and heats it, and a ‘reverse shock’ does the same to the ejecta. The γ -ray burst itself is thought to owe its multi-peaked light curve to a series of ‘internal shocks’ that develop in the relativistic ejecta before they collide with the ambient medium. The heated gas is presumed to form relativistic electrons and magnetic fields with energy densities near equipartition, i.e., similar to that of the gas, and then emit synchrotron radiation². As the forward shock is weighed down by increasing amounts of swept-up material it becomes less relativistic, and produces a slowly fading ‘afterglow’ of X rays, then UV/optical/IR, and then mm and radio radiation.

Mészáros & Rees³ and Sari & Piran⁴ pointed out that when the external shock first forms, optical emission of ~ 9 -14th magnitude from a reverse shock will be visible during or soon after the high-energy burst produced by the internal shocks. Other models have been made which lead to an optical brightness of ~ 18 th magnitude during the γ -ray burst⁵.

Multi-wavelength observations during and immediately after the burst are necessary to detect the emissions from the different regions postulated by these models and transitions between them.

The X-ray emission observed with BeppoSAX during the tails of γ -ray bursts is consistent with extrapolations backward in time of the X-ray afterglow detected many hours later^{6–10}, suggesting that the prompt X-ray emission merges smoothly into the afterglow. On the other hand, HEAO-1 observed serendipitously a prompt X-ray signal in GRB 780506 which disappeared and then reappeared after a few minutes, suggesting a gap between the prompt emission and the afterglow¹¹.

The ROTSE detection¹² of prompt optical emission during and immediately after GRB 990123 shows that optical observations can address the question of which physical region is radiating when. The first ROTSE exposure occurred during the main peak of the burst; weaker γ -ray emission was also present during the second and third ROTSE exposures, but was no longer detected in subsequent exposures.

We here present an extensive set of multi-wavelength observations for GRB 990123, which cover the γ -ray to radio range and permit an analysis of the relation of the burst’s prompt emission to its afterglow in the context of the ‘fireball’ model.

2. OBSERVATIONS

2.1. Prompt γ -ray emission

In Fig. 1 we show the BATSE light curves of GRB 990123 in two energy bands. The burst profile is dominated by two peaks, each lasting about 8 seconds (FWHM), separated by 12 seconds, followed by a shoulder lasting some 40 seconds. The low-energy emission persists longer than the high-energy emission, i.e., GRB 990123 presents a typical case of “hard-to-soft” spectral evolution¹³. Particularly striking is the paucity of > 300 keV emission during the shoulder. The T_{90} duration of the burst¹⁴, as measured in the 50 - 300 keV range is 63.30 ± 0.26 seconds.

Using the BATSE data, we find for the peak flux (50–300 keV) and total fluence (> 20 keV) values of $F_{\text{max}} = 3.8 \times 10^{-6} \text{ erg cm}^{-2} \text{ s}^{-1}$, and $E_b = 3.0 \times 10^{-4} \text{ erg cm}^{-2}$. The redshift ($z = 1.61$) of the optical afterglow, obtained from Fe and Mg absorption lines¹⁵ implies a minimum luminosity distance of 11 Gpc, and a total rest-frame (> 20 keV) γ -ray energy of $4 \times 10^{54} \text{ erg}$, using $H_0 = 70 \text{ km s}^{-1} \text{ Mpc}^{-1}$, and $\Omega_0 = 0.3$ and assuming isotropic emission. To investigate the relation between the optical emission detected with ROTSE and the

γ -ray burst we made spectral fits to the γ -ray data during the time intervals corresponding to the first three ROTSE images. Fig. 2 compares our gamma-ray fits to the simultaneous optical observations by ROTSE. Extending the low-energy power-law to optical frequencies, even allowing for the slope uncertainties, we find that in all three spectra the optical points fall well above the low-energy extension of the γ -ray spectrum, independent of the slope of the latter.

2.2. Multi-wavelength afterglow emission

We observed the afterglow of GRB 990123 in optical, infra-red, sub-mm, mm and radio passbands (see Tables 1, 2 and 3). The optical R-band light curve after the first 0.1 day is well described by a power law decay, $F_\nu = F_0 \cdot t^\alpha$ (t is the time since the burst): we find $\alpha = -1.12 \pm 0.03$ ($\chi_r^2 = 30/28$). To account for the presence of light from the underlying host galaxy¹⁶ we have also fit a model consisting of a power-law decay plus a constant flux; we find $\alpha = -1.14 \pm 0.03$ and $R_{\text{host}} > 24.9$ ($\chi_r^2 = 30/27$). The infra-red observations show a decay that is consistent with that in the R-band; $\alpha_H = -0.94 \pm 0.22$ and (from Ref. 17) $\alpha_K = -1.14 \pm 0.08$. The late-time power law decay connects smoothly with the last three data points of the ROTSE observations (Fig. 3), but not with the first three: the slope of the light curve before these three points is much steeper.

We detect the radio afterglow at 4.88 GHz at the improved optical position¹⁸, using the Westerbork radio telescope. An r.m.s.-noise weighted flux density average gives $F_{4.88\text{GHz}} = 118 \pm 40 \mu\text{Jy}$ (average epoch January 24.46 UT). After January 26 we do not detect the source at 4.88 GHz ($F_{4.88\text{GHz}} = -7 \pm 31 \mu\text{Jy}$; weighted average of the January 26, 28 and 29 data). Similar behavior was observed¹⁹ at 8.46 GHz: initially the source was not detected ($< 68 \mu\text{Jy}$; 2σ ; January 23.63 UT), then it was detected ($260 \pm 32 \mu\text{Jy}$; January 24.65 UT) and not detected after January 26. Such radio behavior is unique, both for its early appearance as well as its rapid decline. The source was not detected at 1.38, 15, 85, 140, 225, 350 and 670 GHz (see Table 2).

We have reconstructed the radio to X-ray afterglow spectrum on January 24.65 UT (see Fig. 4). This interval was selected for the long wavelength coverage possible at the only time of radio detections. Describing the spectrum by a power law ($F_\nu \propto \nu^\beta$) we find that in the optical range $\beta = -0.75 \pm 0.23$, between the optical and X-ray wavebands the spectral slope is $\beta = -0.67 \pm 0.02$, while in the radio range the spectrum rises as $\beta = +1.4 \pm 0.7$.

3. DISCUSSION

Among the six GRBs with known redshifts one other (GRB 980329) has a total energy (assuming isotropic emission) in excess of 10^{54} erg²⁰. Of course, beaming of the γ -ray emission (i.e., strongly anisotropic emission) may make the total energy substantially smaller, and until we have a good understanding of beaming the total energy is not a severe constraint on theoretical models of the initial explosion.

If one assumes that the ROTSE emission comes from a non-relativistic source of size ct , then we can obtain a lower limit to the brightness temperature since the restframe T_b cannot exceed the Compton limit of 10^{12} K. The observed $T_b \gtrsim 10^{17}$ K, is a factor Γ^3 times the restframe value, which means that the bulk Lorentz factor, $\Gamma \gtrsim 50$, confirming the highly relativistic nature of the GRB source. In view of this, and the independent evidence^{2,21,22} that GRBs and their afterglows are emitted by relativistic shocks, we will discuss our results in terms of this ‘fireball’ model.

The ROTSE observations¹² have shown that the prompt optical and γ -ray light curves do not track each other. We show that the prompt optical emission detected with ROTSE during GRB 990123 is not a simple extrapolation of the γ -ray burst to much lower energies, but that there is a smooth connection between the optical emission measured 4.5 minutes after the burst and the afterglow detected later.

The reverse shock could cause emission^{3,4} that peaks in the optical waveband and is observed only during or just after the γ -ray burst, because the shock takes of order the duration of the burst to travel through the ejecta and then stops emitting quickly. The observed properties of GRB 990123 appear to fit this model quite well. If this interpretation is correct, GRB 990123 would be the first burst in which all three emitting regions have been seen: internal shocks causing the γ -ray burst, the reverse shock causing the prompt optical flash, and the forward shock causing the afterglow. The relatively smooth connection between the prompt optical emission and the afterglow fits the expectation that the reverse and forward shock start at about the same time. This model requires roughly equipartition magnetic fields in the ejecta, as does the prompt γ -ray emission.

The radio emission of GRB 990123 is unique both due to its very early appearance and its rapid decline. A look at the broad-band spectrum on Jan 24.65 (Fig. 4) reveals why this was so: it is a power law connecting the X-ray to optical wavebands, which peaks in the several tens of GHz range and turns over towards even lower frequencies. The synchrotron peak frequency does not fall very much above, or is even below, the radio waveband. This location is very different from that of GRB 970508, for which the peak was still in the mm region after 12 days², and that of GRB 971214, for which the peak was in the optical/near

infra-red waveband after 0.6 days²³. We infer from this that the synchrotron peak frequency may span a large range in γ -ray burst afterglows. The rapid decline of the radio flux, caused by the low value of ν_m , may explain why some γ -ray bursts are not detected at radio wavelengths.

Regardless of the location of the peak, the steeply rising radio spectrum implies that the self-absorption frequency, $\nu_a \sim 30$ GHz, similar to earlier bursts. In relativistic blast wave models²⁴ the flux at the peak is constant during the blast wave evolution, although the peak frequency decreases rapidly, as $t^{-3/2}$. In Fig 4. two possible low frequency extrapolations are shown. Both have a self-absorption frequency, ν_a , close to the radio, but the lower one still has a synchrotron peak frequency, $\nu_m > \nu_a \sim 30$ GHz, so that there is an optically thin synchrotron regime, where the spectrum follows the standard low-frequency power law $F_\nu \propto \nu^{1/3}$. This implies that the radio flux should still rise after Jan 24.65, clearly inconsistent with the non-detections a few days after Jan 24.65. The second possibility is that $\nu_m < \nu_a$ already on Jan. 24.65; then the flux at frequencies at and below ν_a would follow the optical decline if ν_a were constant. However, ν_a now begins to fall somewhat as well, and this will lessen the rate of decline at frequencies below ν_a (very much below ν_a it even rises). Here we estimate that on Jan 24.65 the synchrotron peak frequency was at about 30 GHz, as was ν_a , causing a decline of the VLA and WSRT fluxes approximately as $t^{-0.9}$. The first non-detections by the VLA¹⁹ and WSRT after their respective detections are consistent with that decay rate.

The peak flux on Jan. 24.65 (Fig. 4) is less than 2 mJy, while the last three ROTSE exposures have fluxes of ~ 10 mJy. If these exposures captured the early afterglow, the peak flux apparently decreased between 7.5 minutes and ~ 1.2 days after the burst, contrary to the prediction of a constant peak flux during the blast wave evolution. There are, however, several possible explanations for the apparent decrease of the peak flux. If the peak frequency is less than the self-absorption frequency ν_a , then the peak flux will be lowered relative to its unabsorbed value. Or part of the ROTSE flux could be due to a decaying prompt optical component and thus the afterglow component at $t = 7.5$ min. could be less than 10 mJy. Finally, the afterglow peak flux may truly decay with time. The data, therefore, do not allow a strong distinction between a constant and a decreasing peak flux of the afterglow spectrum.

A comparison of GRB 990123 with other well-studied GRBs suggests some patterns. The cooling frequency of GRB 970508, which separates quickly cooling synchrotron electrons from slowly cooling ones, was in the optical/near infra-red after 1.5 days². For GRB 990123 and all other bursts in which the optical-to-X-ray afterglow spectrum could be reconstructed for the few days after the burst, any cooling break was located at or above X-ray frequencies.

Both a higher cooling frequency and a lower peak frequency can be explained by a difference in one shock parameter: the magnetic field in the forward shock region. The lower field also causes a lower peak flux^{24,25}, which with the low peak frequency conspires to make the radio emission weak and brief. The field energy density for the radio-quiet GRB 971214 is estimated to be less than 10^{-5} times the equipartition value, and more than 1000 times weaker than in GRB 970508²⁵; the value for GRB 990123 may be as low as 10^{-6} times equipartition. This suggests we should distinguish between low-field afterglows, which are short and dim in radio, and high-field afterglows, which are bright and long-lived in radio. The absence of detected radio emission in previous bursts with afterglows can then be explained by assuming they were low-field afterglows. We conjecture that such differences in field strength reflect differences in energy flow from the central engine, e.g., in the form of a Poynting wind.

The United Kingdom Infra-Red Telescope is operated by the Joint Astronomy Centre on behalf of the U.K. Particle Physics and Astronomy Research Council. Observations at the Wise Observatory are supported by the Basic Science Foundation of the Israeli Academy of Sciences. The JCMT is operated by the Joint Astronomy Centre on behalf of the UK Particle Physics and Astronomy Research Council, the Netherlands Organisation for Pure Research, and the National Research Council of Canada. We thank G. Watt, I. Robson, and J. van der Hulst for authorizing the JCMT observations. We wish to thank Peter Meikle, Paul Smith, Di Harmer and the KPNO GRB team for their observations, and George Jacoby for providing BVRI photometric standards. TJG is supported by NFRA, PMV by the NWO Spinoza grant. CK, DLB, KH and MSB are supported by NASA.

References

1. Piran, T. Gamma-Ray Bursts and the Fireball Model. *Physics Report* (in the press); preprint <http://xxx.lanl.gov>, astro-ph/9810256
2. Galama, T.J. *et al.* The radio-to-X-ray spectrum of GRB 970508 on 1997 May 21.0 UT. *Astrophys. J.* **500**, L97-L101 (1998).
3. Mészáros, P. and Rees, M.J. Optical and long-wavelength afterglow from gamma-ray bursts. *Astrophys. J.* **476**, 232-237 (1997).
4. Sari, R. & Piran, T. Predictions for the very early afterglow and the optical flash. preprint <http://xxx.lanl.gov>, astro-ph/9901338 (1998).
5. Katz, J.I. Low-frequency spectra of gamma-ray bursts. *Astrophys. J.* **432**, L107-L109 (1994).
6. Costa, E. *et al.* Discovery of an X-ray afterglow associated with the γ -ray burst of 28

February 1997. *Nature* **387**, 783-785 (1997).

7. Feroci, M., *et al.* BeppoSAX follow-up search for the X-ray afterglow of GRB 970111. *Astron. Astrophys.* **332**, L29-L32 (1998).

8. in 't Zand, J.J.M, *et al.* Gamma-Ray Burst 980329 and its X-ray afterglow. *Astrophys. J.* **505**, L119-L122 (1998).

9. Nicastro, L., *et al.* BeppoSAX observations of GRB 970402. *Astron. Astrophys.* **338**, L17-L20 (1998).

10. Piro, L., *et al.* Evidence for a late-time outburst of the X-ray afterglow of GB970508 from BeppoSAX *Astron. Astrophys.* **331**, L41-L44 (1998).

11. Connors, A. & Hueter, G.J. The X-ray characteristics of a classical gamma-ray burst and its afterglow. *Astrophys. J.* **501**, 307-324 (1998).

12. Akerlof, C.W. and McKay, T.A. *Nature* (in the press) (1999).

13. Ford, L.A. *et al.* BATSE observations of gamma-ray burst spectra. 2: Peak energy evolution in bright, long bursts. *Astrophys. J.* **439**, 307-321 (1995).

14. Kouveliotou, C. *et al.* Identification of two classes of gamma-ray bursts. *Astrophys. J.* **413**, L101-L104 (1993).

15. Kelson, D.D. *et al.* *IAU Circ.* No. 7096 (1999).

16. Fruchter, A. *et al.* *GCN Circ.* No. 255 (1999).

17. Bloom, J.S. *et al.* *GCN Circ.* No. 240 (1999).

18. Bloom, J.S., Gal, R.R., Lubin, L.L. Mulchaey, J., Odewahn, S.C., Kulkarni, S.R. *GCN Circ.* No. 206 (1999).

19. Kulkarni, S.R., Frail, D.A. *GCN Circ.* No. 239 (1999).

20. Fruchter, A. Was GRB 980329 at $z \sim 5$? *Astrophys. J.* (in the press); preprint <http://xxx.lanl.gov>, astro-ph/9810224 (1998).

21. Waxman, E. Angular size and emission timescales of relativistic fireballs. *Astrophys. J.* **491**, L19-L22 (1997)

22. Wijers, R. A. M. J., Rees, M. J., and Mészáros, P. Shocked by GRB 970228: the afterglow of a cosmological fireball *Mon. Not. R. Astron. Soc.* **288**, L51-L56 (1997)

23. Ramaprakash, A.N. *et al.* The energetic afterglow of the γ -ray burst of 14 December 1997. *Nature* **393**, 43-46 (1998).

24. Sari, R., Piran, T. & Narayan, R. Spectra and light curves of gamma-ray burst afterglows. *Astrophys. J.* **497**, L17-L20 (1998).
25. Wijers, R.A.M.J. & Galama, T.J. Physical parameters of GRB 970508 and GRB 971214 from their afterglow synchrotron emission. *Astrophys. J.* (in the press); preprint <http://xxx.lanl.gov>, astro-ph/9805341 (1998).
26. Band, D. *et al.* BATSE observations of gamma-ray burst spectra. I - Spectral diversity. *Astrophys. J.* **413**, 281-292 (1993).
27. Gal, R.R., Odewahn, S.C., Bloom, S.J., Kulkarni, S.R., Frail, D.A. *GCN Circ.* No. 207 (1999)
28. Garnavich, P., Jha, S., Stanek, K., Garcia, M. *GCN Circ.* No. 215 (1999)
29. Masetti, N., Palazzi, E., Pian, E., Frontera, F., Barolini, C., Guarnieri, A., P iccioni, A., Valentini, G., Costa, E. *GCN Circ.* No. 233 (1999)
30. Sokolov, V., Zharikov, S., Nicastro, L., Feroci, M., Palazzi, E. *GCN Circ.* No. 209 (1999).
31. Zhu, J., Chen, J.S. and Zhang, H.T. *GCN Circ.* No. 217 (1999).
32. Yadigaroglu, I.A., Halpern, J.P., Uglesich, R., Kemp, J. *GCN Circ.* No. 242 (1999).
33. Yadigaroglu, I.A., Halpern, J.P., Uglesich, R., Kemp, J. *GCN Circ.* No. 248 (1999).
34. Frail, D.A., Kulkarni, S.R., *GCN Circ.*, No. 211 (1999).
35. Heise, J. *et al.* *IAU Circ.* No. 7099 (1999).
36. Bessell, M.S. UBVRI photometry. II - The Cousins VRI system, its temperature and absolute flux calibration, and relevance for two-dimensional photometry. *Publ. Astron. Soc. Pacif.* **91**, 589-607 (1979).
37. Bessell, M.S. and Brett, J.M. JHKLM photometry - Standard systems, passbands, and intrinsic colors. *Publ. Astron. Soc. Pacif.* **100**, 1134-1151 (1988).
38. Schlegel, D.J., Finkbeiner, D.P. and Davis, M. Maps of Dust Infrared Emission for Use in Estimation of Reddening and Cosmic Microwave Background Radiation Foregrounds. *Astrophys. J.* **500**, 525-553 (1998).
39. Granot, J., Piran, T. and Sari, R. Synchrotron Self Absorption in GRB Afterglow *Astrophys. J.* (in the press); preprint <http://xxx.lanl.gov>, astro-ph/9808007 (1999).
40. Baars, J.W.M., Genzel, R., Pauliny-Toth, I.I.K., Witzel, A. The absolute spectrum of

- Cas A - An accurate flux density scale and a set of secondary calibrators. *Astronomy & Astrophysics* **61**, 99-106 (1977).
41. Guilloteau S. *et al.* The IRAM interferometer on Plateau de Bure. *Astronomy & Astrophysics* **262**, 624-633 (1992).
42. Baars, J.W.M., Hooghoudt, B.G., Mezger, P.G., De Jonge, M.J., The IRAM 30-m millimeter radio telescope on Pico Veleta, Spain. *Astronomy & Astrophysics* **175**, 319-326 (1987).
43. Reuter H.-P. and Kramer C. The mm-to-submm continuum spectra of W 3(OH) and K 3-50A. *Astronomy & Astrophysics* **339**, 183-186 (1998).
44. Greve, A., Neri, R. and Sievers, A. The gain-elevation correction of the IRAM 30-m telescope. *Astronomy & Astrophysics Suppl.* **132**, 413-416 (1998).
45. Holland, W. S., et al. SCUBA: A common-user submillimetre camera operating on the James Clerk Maxwell Telescope. *Mon. Not. R. Astron. Soc.* (in the press); preprint <http://xxx.lanl.gov>, astro-ph/9809122 (1999).
46. Smith, I. A., et al. SCUBA sub-millimeter observations of gamma-ray bursters I. GRB 970508, 971214, 980326, 980329, 980519, 980703. *Astronomy & Astrophysics* (in the press); preprint <http://xxx.lanl.gov>, astro-ph/9811026 (1999).
47. Landolt, A.U., UBVRI photometric standard stars in the magnitude range 11.5 < V < 16.0 around the celestial equator. *Astron. J.* **104**, 340-376 (1992).
48. Casali, M.M. and Hawarden, T.G. JCMT-UKIRT Newsletter, No. 3, 33 (1992)

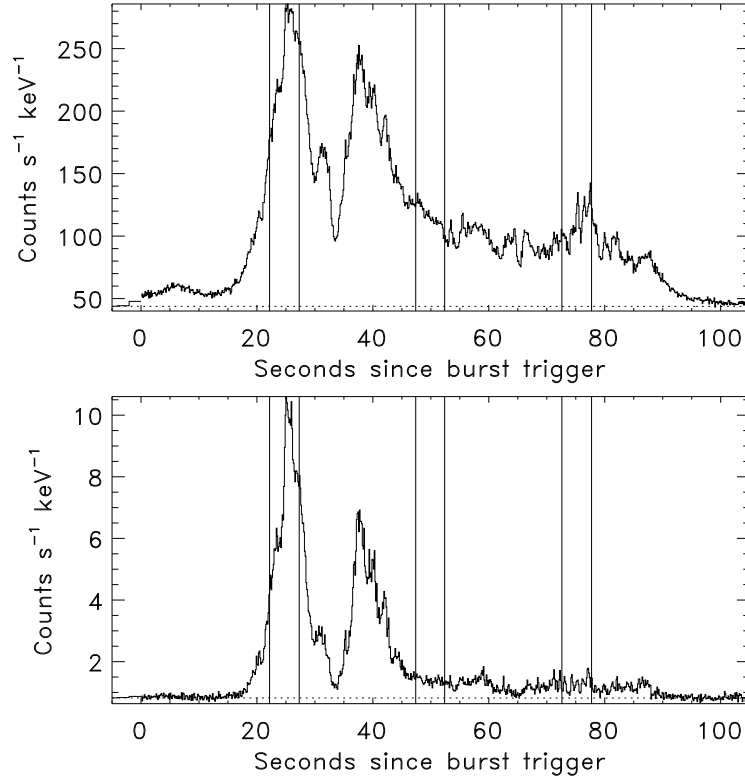


Fig. 1.— The two panels show the BATSE light curves of GRB 990123 in two energy ranges, 25–230 keV (top) and 320–1800 keV (bottom). Times are relative to the BATSE trigger time of UT 9h 46m 56.1s on January 23. The vertical lines indicate the time intervals of the first three ROTSE observations¹².

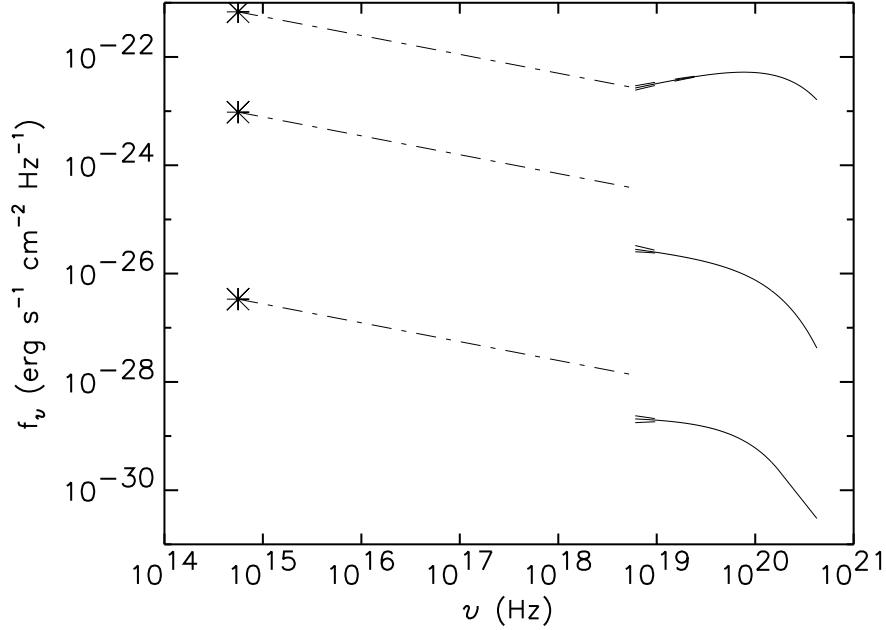


Fig. 2.— Optical flux and gamma-ray spectra for the time intervals of the 3 ROTSE observations. The gamma-ray curves (solid) are fits to BATSE spectra using the Band function²⁶, which consists of a low-energy power law with an exponential cutoff which merges smoothly with a high-energy power law. The curves for the first (third) time interval have been shifted up (down) by a factor of 1000. The data point on the left is the reported ROTSE magnitude converted into a flux density in the middle of the V band. The dashed curves on the low energy end of the gamma-ray spectra show the 3σ variations in the low energy spectral index. The dot-dashed curves are the extrapolation of the optical flux to the X-ray band using the power law which connects the observed optical and lowest-energy γ -ray fluxes for the first ROTSE time interval.

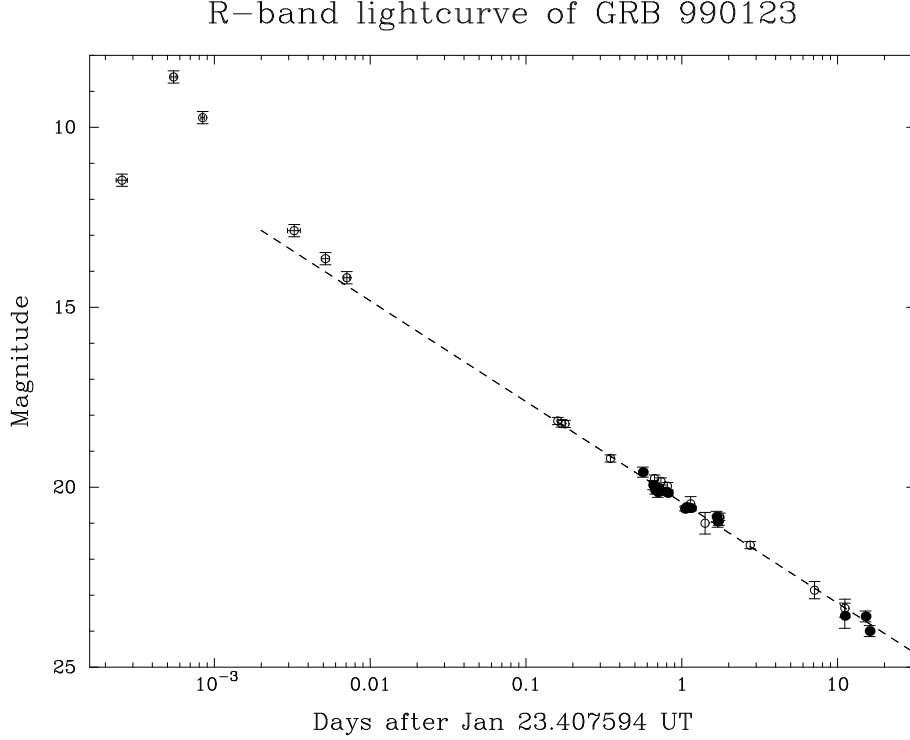


Fig. 3.— R-band light curve of the afterglow of GRB 990123. The filled circles indicate results of our observations. The open circles are data taken from Refs 27-33: we determined the corresponding magnitude for our calibration. The dashed line indicates a power law fit to the light curve (for $t > 0.1$ days), which has exponent -1.12 ± 0.03 . Also included are the ROTSE data¹². ROTSE uses an unfiltered CCD, but an equivalent V band magnitude is reported; here we adopted a 0.1m error for the ROTSE data points and assuming a constant color we have applied a color correction of $V-R = 0.35 \pm 0.14$. The power law fit is extrapolated backward; it gives a splendid description of the last three ROTSE data points.

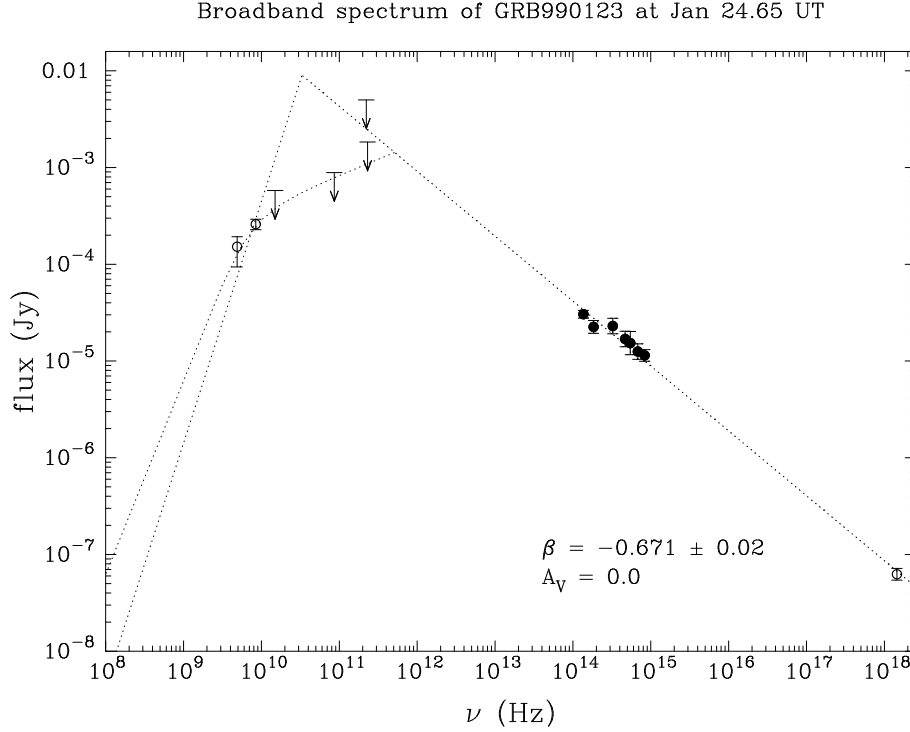


Fig. 4.— The spectral flux distribution of the afterglow at 1999 January 24.65 UT. Shown are the WSRT 4.88 GHz detection (this paper), the VLA 8.46 GHz detection³⁴, the KPNO 4-m U band, WIYN B,V,R and I and UKIRT H observations (this paper), the K band detection¹⁷, and the X-ray (2-10 keV) flux³⁵. Also shown are the Ryle 15 GHz, PdBI 86 and 230 GHz and the JCMT 220 GHz 2- σ upper limits (this paper; we scaled these values back to the central time of the epoch by assuming that the source flux exhibits a $t^{-1.1}$ decay, i.e., we used conservative limits). The photometric calibration has been taken from Ref. 36 for B, V, R and I and Ref. 37 for H. We corrected the optical fluxes for Galactic foreground absorption ($A_V = 0.053$, as inferred from the dust maps of Ref. 38). If more than one value per filter was available around the central time of the epoch, we took their weighted average. All values were brought to the same epoch by applying a correction using the slope of the fitted light curve. We fitted the resulting optical to X-ray spectral flux distribution with a power law and an exponential optical extinction law, $F_\nu \propto \nu^\beta e^{-\tau}$, where we assume that the extinction optical depth, $\tau \propto \nu$. The fit provides a negative extinction ($A_V < 0.19$; 90 % confidence) and was subsequently fixed at zero. We find $\beta = -0.67 \pm 0.02$ ($A_V = 0$; $\chi_r^2 = 6/7$); indicated is the resulting fit. Also shown for reference are two possible extrapolations of the low-frequency part of the spectrum: (i) a self-absorbed spectrum $F_\nu = F_{\nu_a}(\nu/\nu_a)^2(1 - \exp[-(\nu/\nu_a)^{-5/3}])$ (Ref 39), for a self-absorption frequency, $\nu_a = 7.5$ GHz and a flux density, $F_{\nu_a} = 350 \mu\text{Jy}$, and (ii) the classic spectrum of a self-absorbed radio source with asymptotic spectral index $+5/2$. Note that realistic spectra are much rounder at the peak than the simple broken power law spectra shown (see the discussion for the details).

Optical and Infra-red observations of GRB 990123				
UT date (1999 Jan)	magnitude	filter	exp. time (seconds)	telescope/reference
Jan 23.970	19.58 ± 0.14	R	3600	UPSO 1-m
Jan 24.028	20.42 ± 0.10	B	3000	UPSO 1-m
Jan 24.999	21.82 ± 0.12	B	3600	UPSO 1-m
Jan 25.029	21.14 ± 0.16	V	600	UPSO 1-m
Jan 24.066	20.38 ± 0.26	B	120	Wise 1-m
Jan 24.062	19.94 ± 0.13	R	600	Wise 1-m
Jan 24.081	20.08 ± 0.11	R	600	Wise 1-m
Jan 24.110	20.14 ± 0.14	R	600	Wise 1-m
Jan 24.116	20.02 ± 0.09	R	600	Wise 1-m
Jan 25.079	20.82 ± 0.15	R	900	Wise 1-m
Jan 25.092	21.75 ± 0.21	B	1200	Wise 1-m
Jan 25.105	20.95 ± 0.16	R	900	Wise 1-m
Jan 24.198	20.12 ± 0.06	R	1000	JKT
Jan 24.210	20.14 ± 0.05	R	1000	JKT
Jan 24.222	20.16 ± 0.06	R	1000	JKT
Jan 24.456	20.60 ± 0.06	R	900	WIYN
Jan 24.477	20.55 ± 0.04	R	600	WIYN
Jan 24.487	20.14 ± 0.08	I	600	WIYN
Jan 24.496	20.89 ± 0.06	V	600	WIYN
Jan 24.505	21.21 ± 0.04	B	600	WIYN
Jan 24.515	20.57 ± 0.04	R	600	WIYN
Jan 24.544	20.96 ± 0.08	V	600	WIYN
Jan 24.553	20.58 ± 0.05	R	600	WIYN
Feb 3.519	23.57 ± 0.35	R	900	WIYN
Feb 3.533	> 22.8	I	900	WIYN
Feb 7.513	23.59 ± 0.15	R	3500	WIYN
Feb 8.460	24.00 ± 0.15	R	3600	WIYN
Jan 24.497	20.34 ± 0.10	U	900	KPNO 4-m
Jan 24.660	19.14 ± 0.13	H	1020	UKIRT
Jan 27.660	20.39 ± 0.26	H	1080	UKIRT

Table 1: The log of the optical and infra-red observations. Eight reference stars (see Table 3) were used to obtain the differential magnitude of the optical transient (OT) in each observation. Telescopes: WIYN 3.5-m telescope at Kitt Peak (WIYN), Uttar Pradesh State Observatory 1-m telescope (UPSO 1-m), Wise Observatory 1-m telescope (Wise 1-m), Jakobus Kapteyn Telescope, La Palma (JKT), Kitt Peak National Observatory 4-m Mayall telescope (KPNO 4-m), United Kingdom Infra-Red Telescope, Hawaii (UKIRT). Instruments and CCDs used: UPSO 1-m: CCD Camera, 512×512 CCD, $0.76''/\text{pixel}$; Wise 1-m: TEK $1k \times 1k$ CCD, $0.70''/\text{pixel}$; JKT: TEK $2k \times 2k$ CCD, $0.33''/\text{pixel}$; WIYN: TEK $2k \times 2k$ CCD, $0.197''/\text{pixel}$; KPNO 4-m: $8k \times 8k$ CCD Mosaic Camera, $0.258''/\text{pixel}$; UKIRT: IRCAM3 with FPA42 256×256 detector, $0.29''/\text{pixel}$.

Radio and (sub) mm observations of GRB 990123

Freq	UT date 1999 (central)	duration (hours)	flux microJansky	Reference
1.380	Jan 27.20	8.4	37 ± 22	WSRT
4.88	Jan 24.28	12	104 ± 42	WSRT
4.88	Jan 25.47	2.9	164 ± 100	WSRT
4.88	Jan 26.29	1.4	-65 ± 130	WSRT
4.88	Jan 28.27	12	-3 ± 41	WSRT
4.88	Jan 29.17	7.4	-9.3 ± 55	WSRT
4.88	Jan 30.27	12	-74 ± 44	WSRT
4.88	Jan 31.26	12	20 ± 41	WSRT
4.88	Feb 6.25	12	30 ± 44	WSRT
4.88	Feb 7.13	6.7	112 ± 85	WSRT
8.46	Jan 23.63		$<68 (2\sigma)$	VLA
8.46	Jan 24.65		260 ± 32	VLA
8.46	Jan 26		$<78 (2\sigma)$	VLA
8.46	Jan 27		$<50 (2\sigma)$	VLA
8.46	Jan 28		$<50 (2\sigma)$	VLA
15.0	Jan 25.26	9.9	160 ± 180	Ryle
15.0	Jan 26.27	10.4	-12 ± 180	Ryle
15.0	Jan 29.20	6.4	-197 ± 200	Ryle
15.0	Jan 30.40	3.7	106 ± 420	Ryle
15.0	Jan 31.39	3.8	48 ± 300	Ryle
15.0	Feb 4.39	3.6	378 ± 270	Ryle
15.0	Feb 6.37	4.1	-140 ± 300	Ryle
15.0	Feb 8.36	2.8	-16 ± 280	Ryle
86.27	Jan 25.18	4.5	$(1.0 \pm 2.9) \times 10^2$	PdBI
232.0	Jan 25.18	4.5	$(-1.6 \pm 1.2) \times 10^3$	PdBI
86.27	Feb 1.47	4.5	$(-5.0 \pm 3.1) \times 10^2$	PdBI
212.6	Feb 1.47	4.5	$(0.4 \pm 1.3) \times 10^3$	PdBI
86.27	Feb 4.06	3.5	$(-0.3 \pm 4.8) \times 10^2$	PdBI
231.5	Feb 4.06	3.5	$(-2.7 \pm 4.3) \times 10^3$	PdBI
86.64	Jan 28.54	0.42	$(-4.1 \pm 9.1) \times 10^3$	Pico Veleta
142.3	Jan 28.54	0.42	$(-3.7 \pm 3.3) \times 10^4$	Pico Veleta
228.9	Jan 28.54	0.42	$(-0.9 \pm 1.9) \times 10^4$	Pico Veleta
86.64	Jan 30.53	1.42	$(8.5 \pm 3.5) \times 10^3$	Pico Veleta
142.3	Jan 30.53	1.42	$(1.0 \pm 2.9) \times 10^4$	Pico Veleta
228.9	Jan 30.53	1.42	$(1.3 \pm 1.2) \times 10^4$	Pico Veleta
222	Jan 24.68	0.65	$(-4.1 \pm 2.5) \times 10^3$	JCMT ¹
222	Jan 27.83	0.62	$(0.7 \pm 1.9) \times 10^3$	JCMT ¹
353	Jan 27.89	1.25	$(-3.3 \pm 1.2) \times 10^3$	JCMT ¹
353	Jan 29.88	1.0	$(0.8 \pm 1.5) \times 10^3$	JCMT ¹
353	Feb 4.83	0.7	$(4.9 \pm 1.5) \times 10^3$	JCMT ¹
353	Feb 5.85	1.5	$(1.2 \pm 1.1) \times 10^3$	JCMT ¹
666	Jan 27.88	1.0	$(-0.2 \pm 1.7) \times 10^4$	JCMT ^{1,2}
666	Jan 29.87	0.75	$(-0.8 \pm 2.3) \times 10^4$	JCMT ^{1,2}
666	Feb 4.82	0.5	$(1.5 \pm 1.8) \times 10^4$	JCMT ^{1,2}

Table 2: Summary of the radio and (sub) mm observations of GRB 990123. Westerbork Synthesis Radio Telescope (WSRT): We used the Multi-Frequency Front Ends (MFFE)s¹ at 4.88 and 1.38 GHz, and the DCB continuum correlator, providing us with 8 bands of width 10 MHz at each frequency. The data were calibrated using interleaved observations of 3C 48, 3C 147 and 3C 286⁴⁰. VLA data are taken from Ref. 19. IRAM Plateaux de Bure Interferometer (PdBI)⁴¹: Observations were done in five antenna configurations, on January 25 in 5B1 and on February 1st, in 5B2. Spectral bandwidth of the dual frequency SIS receivers at 86.2 GHz was 560 MHz (LSB tuning), and 310 MHz (DSB tuning) at frequencies above 210 GHz. Good weather conditions allowed to use the atmospheric phase correction system to improve the signal to noise ratio. Results are given for position-fixed point source fits. Pico Veleta: Observations with the IRAM 30-m telescope on the Pico Veleta in Spain⁴² were done at 86.638, 142.33 and 228.930 GHz in wobbler switching mode with SIS receivers connected to the 1 GHz backends. Flux calibration was relative to W3 (OH)⁴³, using the gain-elevation curve from Ref. 44. James Clerk Maxwell Telescope (JCMT): Observations were made using SCUBA⁴⁵ in the photometry mode, as for previous bursts⁴⁶. At 450/850 μ m, GRB 990123 was in the central pixel of the arrays (at 1350 μ m there is only one bolometer). The secondary was chopped between the source and sky at 7 Hz to take out small relative DC drifts between the bolometers and remove large-scale sky variations. The opacity at 450 and 850 μ m was measured from skydips while using the continuously monitored 1.3 mm opacity as a guideline of any trends between the skydips. For the absolute flux calibration the gain was measured using Mars. The 3.3 σ result at 353 GHz on Feb 4.76 UT is presumably a statistical fluctuation, since the result was not confirmed the following day.

1.The “integration” time always refers to the on-source plus off-source time. An 18 sec integration thus amounts to 9 sec on-source observation time. 2. The last 450/850 measurement was excluded from the 450 reduction because of the low elevation of the source.

ID	Δ R.A.('')	Δ Decl.('')	U	B	V	R	I	H
1	-34.30	24.33	15.38 ± 0.01	15.45 ± 0.01	14.88 ± 0.01	14.57 ± 0.01	14.28 ± 0.01	13.54 ± 0.01
2	-92.37	53.94		17.84 ± 0.04	16.83 ± 0.01	16.00 ± 0.01	15.23 ± 0.02	
3	-96.92	48.55	16.88 ± 0.02	16.97 ± 0.02	16.34 ± 0.01	15.93 ± 0.01	15.57 ± 0.01	
4	49.55	30.08			20.34 ± 0.22	19.66 ± 0.37	18.07 ± 0.40	
5	-15.19	-29.00			20.76 ± 0.32	19.76 ± 0.51	19.09 ± 0.55	17.37 ± 0.03
6	23.94	-89.03		19.80 ± 0.23	18.95 ± 0.06	18.56 ± 0.10	18.23 ± 0.13	
7	-30.64	-74.52			19.86 ± 0.15	20.08 ± 0.32	20.09 ± 0.46	
8	64.13	-81.67	16.12 ± 0.01	16.18 ± 0.01	15.52 ± 0.01	15.14 ± 0.01	14.82 ± 0.01	

Table 3: The magnitudes and offset from the OT in arc seconds of the eight comparison stars used. The error listed is the quadratic average of the measurement error (Poisson noise) and the error originating from measuring the OT with respect to several reference stars. Not included is the calibration error, which we estimate to be 0.10. The V, R and I band images were calibrated using JKT images of the Landolt PG1528+062 and SA98 fields⁴⁷. The Landolt star SA104-335, imaged on Feb. 3.21 UT with the JKT, was used for the U band calibration. We also calibrated the GRB field in B, V, R and I with images taken with the KPNO 0.9m, around Feb. 29.07 UT. The V, R and I calibration agrees within 4 percent for the brighter reference stars with the JKT values. We adopt the V, R and I calibration of the JKT and the B of the KPNO 0.9m. For the H band the standard star FS21 (Ref. 48) was observed during the two nights the OT was detected.